The Astrophysical Journal, 733:33 (8pp), 2011 May 20 doi:10.1088/0004-637X/733/1/33

THE EFFECTS OF ELECTRON-BEAM-INDUCED ELECTRIC FIELD ON THE GENERATION OF LANGMUIR TURBULENCE IN FLARING ATMOSPHERES

Valentina V. Zharkova and Taras V. Siversky
Department of Mathematics, University of Bradford, Bradford BD7 1DP, UK; v.v.zharkova@brad.ac.uk, taras.siversky@gmail.com
Received 2010 February 28; accepted 2011 March 16; published 2011 April 29

ABSTRACT

The precipitation of an electron beam injected into the solar atmosphere is studied for the generation of Langmuir wave turbulence in the presence of collisional and Ohmic losses. The system of quasi-linear time-dependent kinetic equations describing the evolution of beams and Langmuir waves is solved by using the summary approximation method. It is found that at upper atmospheric levels the self-induced electric field suppresses the generation of Langmuir turbulence to very small regions below injection. With further precipitation into deeper atmosphere the initial single power-law distributions of beam electrons are transformed into energy distributions with maxima at lower energies formed by collisional and Ohmic energy depletion. The electrons with lower energies ($<$20 keV) generate on large spatial scales intense low-hybrid and high-hybrid Langmuir waves with well-defined patterns in the corona while higher energy electrons generate moderate low-hybrid waves in the chromosphere. The maximum wave density appears at the maximum of the ambient density. The self-induced electric field reduces the level and makes the regions with low-hybrid Langmuir turbulence narrower in the corona and upper chromosphere. The higher the beam energy flux or its self-induced electric field, the narrower the regions with Langmuir turbulence. High-hybrid Langmuir waves in the form of multiple patterns in space (in the corona) and energy (below 20 keV) are found to be generated only by a very intense electron beam. The number of patterns in both dimensions is also shown to be significantly reduced by the self-induced electric field.

Key words: plasmas – scattering – Sun: atmosphere – Sun: flares – Sun: X-rays, gamma rays – turbulence – waves

Online-only material: color figure

1. INTRODUCTION

Precipitation of high energy beam electrons with negative power-law energy distributions with scattering in Coulomb collision with the ambient particles can account for the hard X-ray (HXR) power-law photon spectra often observed in solar flares (Brown 1971; Syrovatskii & Shmeleva 1972). This HXR emission is often accompanied by noticeable type III bursts of radio emission simultaneously observed in flares (Zheleznyakov & Zaitsev 1970; Chernov 2006, and references therein). The latter was first interpreted analytically by a quasi-linear relaxation on the Langmuir turbulence (Zheleznyakov & Zaitsev 1970) or other types of turbulence (Diakonov & Somov 1988) caused by the instability of beam electrons having energy distributions with positive slope, e.g., $\partial f/\partial V > 0$, although the positive slopes below a lower cutoff energy E_0 are difficult to observe in HXR or radio emission since they are obscured by the emission coming from thermal electrons.

Simulations of particle acceleration in a reconnecting current sheet for the likely coronal acceleration mechanism (Zharkova & Gordovskyy 2005) have shown energy/velocity distributions with double exponents. The energy spectra of ejected particles have a positive slope at lower energies and negative slope at higher ones with the maxima occurring at the energies close to the lower cutoff energies in HXR photon spectra. The recent self-consistent particle-in-cell simulations of the particle energy spectra formed in a diffusion reconnection region confirmed a formation of electron energy spectra with a positive slope and occurrence of Langmuir waves at ejection from current sheets (Siversky & Zharkova 2009a). Depending on reconnection scenarios these beams can be injected either as short pulses or as a steady stream of electrons.

Hannah et al. (2009), considering collisional and particle–wave interaction for a short (1 s) impulse of beam electrons with a negative energy slope above the lower cutoff energy combined with a Gaussian distribution for thermal electrons, showed that beam electrons can generate noticeable Langmuir turbulence, which flattens the initial positive slope in the mean electron distributions caused by the resulting "bump-in-tail" distribution of thermal and beam electrons. The authors show this effect to be important for the interpretation of the mean electron spectra deduced from HXR emission and dips appearing in their energy distributions combining both power-law and thermal energy spectra. However, this conclusion needs to be tested for longer injection times since HXR and microwave (MW) emission can last in flares for tens of minutes.

For a steady injection the precipitation of beam electrons into lower atmospheric levels will result in collisional depletion of their single power law energy distributions into energy distributions with positive slopes (Syrovatskii & Shmeleva 1972; Emslie & Smith 1984). These positive slopes can be further enhanced by particle reflection from a magnetic mirror (Leach & Petrosian 1981) or by an electric field induced by the precipitating beam (Knight & Sturrock 1977; McClements 1992; Zharkova & Gordovskyy 2006). These different types of energy losses are found to be important at different depths and/or times of beam precipitation into flaring atmospheres (Siversky & Zharkova 2009b).

First attempts to evaluate turbulence generated at lower atmospheric levels by electron beams with single negative power-law distributions above the lower cutoff energy were made by Emslie & Smith (1984); Hamilton & Petrosian (1987) described analytically particle–wave interaction of beam electrons affected by Coulomb collisions with ambient particles in the atmospheres with static exponential density gradients. The collisions of beam electrons were found to create energy distributions with positive slopes which become unstable and generate very intense Langmuir waves (Emslie & Smith 1984). The particle–wave interaction at any precipitation depth was shown to have a noticeable but not a dominant effect on electron distributions that cannot be observed in HXR or MW emission since the electron energy transferred to the waves is strongly absorbed by the ambient plasma leading to its additional (less than 8%) heating (Hamilton & Petrosian 1987; McClements 1987). At the same time a fusion of two Langmuir waves into a transverse, one at twice the plasma frequency (Emslie & Smith 1984), can produce noticeable gyrosynchrotron emission often observed in flares (Chernov 2006).

More detailed investigation of the role of electron collisions on the generation of plasma waves in converging magnetic loops for different ratios U of the plasma-to-gyrofrequencies showed the appearance of either ordinary (*O*-mode) or extraordinary (*X*-mode) longitudinal plasma waves near the resonance of magneto-ionic modes (Hamilton & Petrosian 1990). For $U < 1$ the resonance occurs with the *O*-mode producing slow plasma waves while for $U > 1$ it occurs for the *X*-mode producing Langmuir waves. The growth rates of these waves were found to decrease strongly with the increase in ambient temperature or the decrease in ratio of the beam-to-ambient density.

McClements (1989) simulated heating of a simple hydrostatic atmosphere by Langmuir waves produced by an electron beam losing energy in collisions, Ohmic losses, and particle–wave processes. He showed that, contrary to findings of Emslie & Smith (1984), the collisional depletion of low energy electrons combined with Ohmic losses does not produce a two-beam instability at any precipitation depth unless electron distributions have already reached the plateau at the acceleration process prior to injection.

However, a steady density gradient assumed for hydrostatic atmospheres by McClements (1989) is not a good assumption for flares, which are very dynamic events, with a sharp increase of density over the transition region (see, for example, Somov et al. 1981; Zharkova & Zharkov 2007). Therefore, given the fact that a stationary injection of electron beams produces a substantial electric field in the corona (Zharkova & Gordovskyy 2006), one question remains. If both collisional and Ohmic losses are considered for dynamic flaring atmospheres, will it still result in the formation of electron energy spectra with positive slopes at deeper levels and the generation of Langmuir waves?

In this paper, we consider the particle–wave interaction of beam electrons during their stationary injection into a flaring atmosphere by taking into account collisional and Ohmic losses for beams with positive energy slopes gained either at acceleration or precipitation. The problem is formulated in Section 2, the method of solution and the results are presented in Section 3, and conclusions are drawn in Section 4.

2. FORMULATION OF THE PROBLEM

An electron beam injected into a flaring atmosphere is represented by electron distribution $f(v, x, t)$, where t is time, x is a one-dimensional coordinate (i.e., depth), and v is the velocity along the x coordinate. Waves are represented by their energy spectra $W(v, x, t)$, where v is the phase velocity of plasma waves; and the meaning of W for waves is identical to the distribution function $f(v, x, t)$ for electrons. By using the quasi-linear approach for interaction between particles and Langmuir waves (Zheleznyakov & Zaitsev 1970; Hamilton & Petrosian 1987) including a self-induced electric field, the simultaneous equations for f and W are solved (McClements 1989):

$$\left(\frac{\partial}{\partial t} + v\frac{\partial}{\partial x}\right) f - \frac{e\mathcal{E}}{m_e} v^2 \frac{\partial}{\partial v}\left(\frac{f}{v^2}\right) = \frac{e^2\omega_p^2}{m_e}\frac{\partial}{\partial v}\left(\frac{\ln v/v_e}{v^2} f\right) + \frac{\pi\omega_p}{m_e n}\frac{\partial}{\partial v}\left(vW\frac{\partial f}{\partial v}\right) + \frac{4\pi e^4 n \ln\Lambda_b}{m_e^2}\frac{\partial}{\partial v}\left(\frac{f}{v^2}\right), \quad (1)$$

$$\left(\frac{\partial}{\partial t} + 3\frac{v_e^2}{v}\frac{\partial}{\partial x}\right) W = e^2\omega_p^2 \frac{\ln v/v_e}{v} f + \frac{\pi\omega_p}{n} v^2 W \frac{\partial f}{\partial v} - \frac{\pi e^4 n \ln\Lambda_p}{m_e^2 v_e^3} W, \quad (2)$$

where n, v_e, and ω_p are density, electron thermal velocity, and plasma frequency of the background plasma; $\ln\Lambda_b$ and $\ln\Lambda_p$ are Coulomb logarithms for beam and plasma electrons, respectively. $\mathcal{E}$ is the self-induced return current electric field, which is calculated as follows (McClements 1992; Siversky & Zharkova 2009b):

$$\mathcal{E}(t, x) = \frac{e}{\sigma(x)} \int_{v_{min}}^{v_{max}} dv v f(v, x, t), \quad (3)$$

where $\sigma(x)$ is the classic conductivity of the ambient plasma.

The distribution function f of an electron beam in the point of injection is taken in the following form (Zharkova & Gordovskyy 2005):

$$f(x = x_{min}, v, t) = f_n \frac{E^\kappa}{E^{\kappa+\delta} + E_0^{\kappa+\delta}}, \quad (4)$$

where $E = m_e v^2/2$ is the electron energy. For energies greater than the energy of the maximum, or lower cutoff energy, E_0, the electron spectrum is a negative power law with the index δ, i.e., $f \propto E^{-\delta}$, while low energy part of the spectrum ($E < E_0$) is positive power law with the index κ.

3. RESULTS AND DISCUSSION

3.1. Method of Solution and Model Parameters

For the electron–wave interaction, the quasi-linear approach is utilized as suggested by Zheleznyakov & Zaitsev (1970) so that Equations (1) and (2) together with Equation (3) are solved numerically using the summary approximation method (Siversky & Zharkova 2009b), taking Equation (4) as the boundary condition. The electron beam is assumed to be steadily injected to deeper atmospheric levels with a single power-law distribution in energy, i.e., $\partial f/\partial E \leqslant 0$, which means that $\kappa = 0$ in Equation (4).

The injected beam parameters are as follows: spectral index at lower energy (before the break) $\kappa = 5$ (used only for a single simulation described in Section 3.2.1), high-energy index (above the break, used in all other simulations) $\delta = 3$ and 7, cutoff energy $E_0 = 12$ keV, energy flux of the beam is $F_0 = (1\text{–}100) \times 10^{10}$ erg cm^{-2} s^{-1}, and low-energy index κ varies from 5 to 0. Density and temperature profiles of the ambient plasma are adopted from the hydrodynamic atmosphere heated by the beam (Zharkova & Zharkov 2007) as shown in Figure 1 for the beam parameters $F_0 = 10^{11}$ erg cm^{-2} s^{-1} and $\delta = 3$.

Most simulations are done for a large-scale simulation region of about 1.5×10^8 cm in a linear distance with the density profile

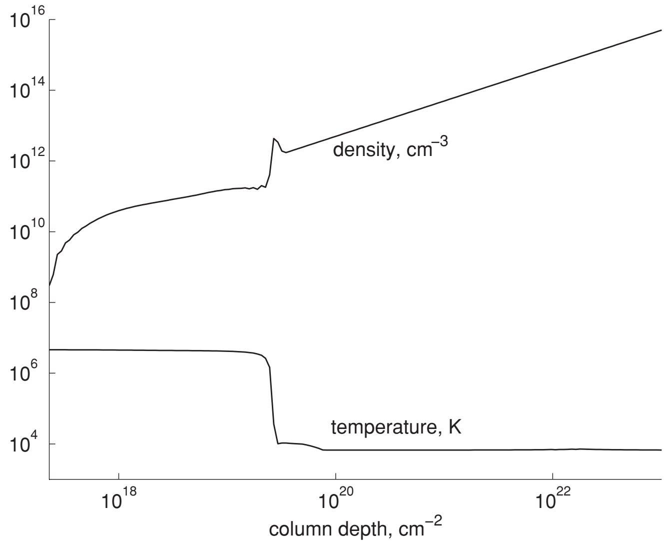

Figure 1. Sample of density and temperature distributions of the ambient plasma calculated by the hydrodynamic model (Zharkova & Zharkov 2007) heated by electron beam with the initial energy flux $F_0 = 10^{11}$ erg cm^{-2} s^{-1} and power-law index $\delta = 3$ of the beam electron distribution.

defined by the hydrodynamic model presented in Figure 1, i.e., from 2.35×10^{17} cm^{-2} to 1×10^{23} cm^{-2} in terms of the column depth. The spatial grid has 200 nodes logarithmically (in terms of the column depth) distributed over the simulation region. So the spatial resolution is variable in terms of the column depth but in terms of a linear distance it is about 7×10^5 cm.

On the other hand, the simulation for the electron beam having double power-law initial distribution with the positive slope below the break energy and negative slope above it (shown in Figure 2) is done for a small-scale region of about 7 cm with the same number of nodes and resolution of about 0.05 cm.

3.2. Electric Field Effects on Langmuir Turbulence

3.2.1. Selection of the Initial Beam Distribution

Let us first select an electron beam injected with the initial energy distributions with a positive slope having index $\kappa = 5$ at energies lower 10 keV (see Equation (4)) predicted by some acceleration models (Zharkova & Gordovskyy 2005; see Figure 2) and explore the Langmuir turbulence it produces.

It turns out that there is fast collisional depletion (flattening) at lower energies of such initial electron distributions (Figure 2, left plot) caused by the fast resonant interaction with Langmuir waves that resembles the findings by Zheleznyakov & Zaitsev (1970) and Hamilton & Petrosian (1990). This depletion occurs at a short distance of 3 cm and a very short timescale of $\sim 3 \times 10^{-8}$ s which is similar to 40 plasma periods obtained by Karlický et al. (2008). This means that with sufficient accuracy the initial distribution for electron beams can be selected with $\kappa = 0$, so we can vary only δ.

3.2.2. Electron Distribution during Precipitation

A hydrodynamic response forms steep gradients and temperature variations at the transition region in the ambient plasma (see Figure 1), which, in turn, forms a maximum in the electric field at this region leading to a significant increase of energy losses by beam electrons in this electric field (Emslie 1980; Zharkova & Gordovskyy 2006; Siversky & Zharkova 2009b) and a strong effect on electron beam distributions and their HXR emission. In particular, the electric field induced by a precipitating beam is shown effectively to decelerate precipitating electrons and to accelerate them upward forming an electric circuit along the whole loop (Zharkova et al. 2010).

It was shown earlier that in a pure collisional precipitation described by continuity equation (Syrovatskii & Shmeleva 1972) an electron beam with negative power-law spectrum gains positive slope at lower energies with the maxima at about $\delta \times E_{\rm low}$ (Zharkova & Gordovskyy 2006). This is different from the results obtained by Hamilton & Petrosian (1987) for small-scale non-homogeneous atmospheres and by McClements (1989) for a hydrostatic atmosphere that can be explained by different physical conditions between hydrostatic and hydrodynamic atmospheres (Somov et al. 1981; Zharkova & Zharkov 2007).

The inclusion of a self-induced electric field is shown to steepen these positive slopes in the electron distributions making them appear at upper precipitation levels compared to pure collisions (Zharkova & Gordovskyy 2006; compare solid and dashed plots in Figure 3). In this case, beam electron density is found to be higher at upper atmospheric levels (in the corona) and lower at lower levels (in the chromosphere), in comparison to pure collisional precipitation of a beam (Zharkova & Gordovskyy 2006; Siversky & Zharkova 2009b; see the left and right plots in Figure 3).

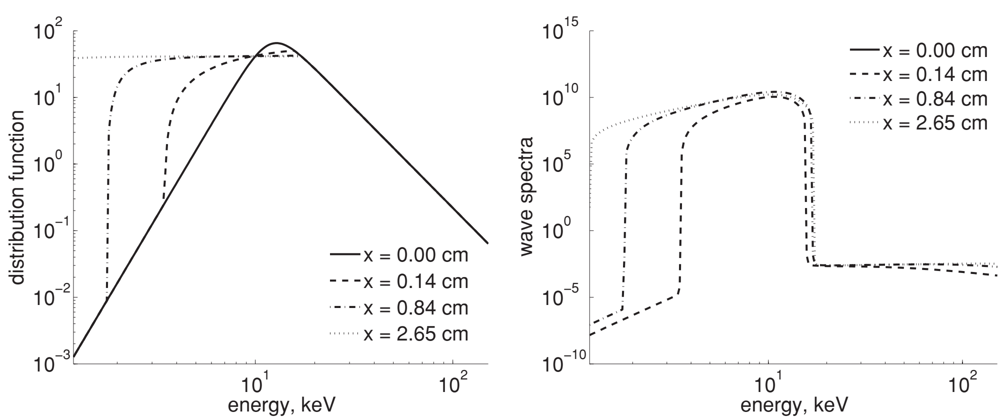

Figure 2. Left plot: distribution function (in arbitrary units) of the beam electrons with spectral index $\delta = 3$ and initial energy flux 10^{11}erg cm^{-2} s^{-1} at various depths from the injection point calculated at 3×10^{-8} s after the injection onset. Right plot: energy spectra (in arbitrary units) of Langmuir waves generated by this electron beam at various depths from the injection point.

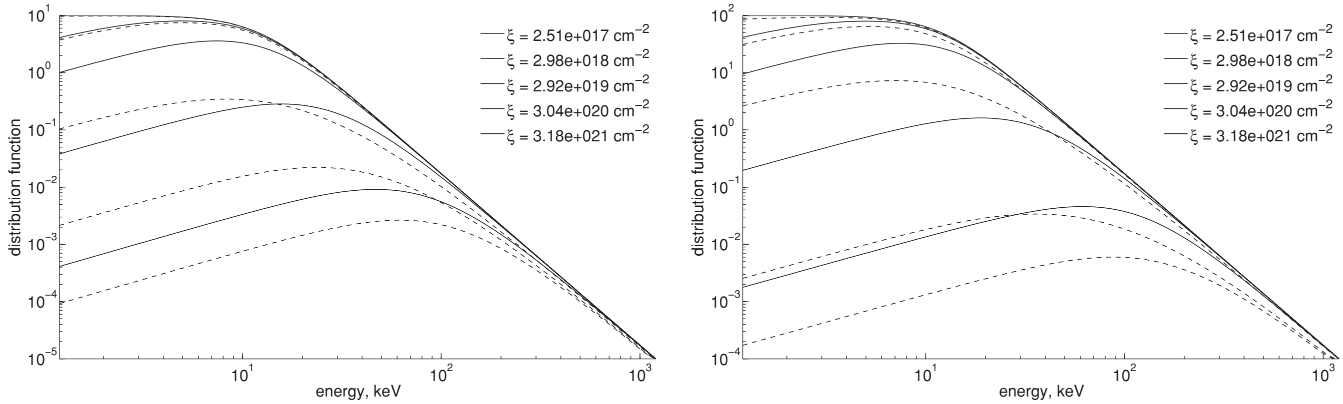

Figure 3. Electron differential distributions (in s cm^{-4}) for collisions without (solid) and with (dashed) electric field for the beams with $\delta = 3$ and $F_0 = 10^{10}$ erg cm^{-2} s^{-1} (left plot) and $F_0 = 10^{11}$ erg cm^{-2} s^{-1} (right plot). The curves are shown from top to bottom for column depths ξ shown in the legend starting from $\xi = 2 \times 10^{17}$ cm^{-2} for the uppermost ones (both solid and dashed).

The presence of such positive slopes in electron distributions leads to the generation of plasma waves in the corona and the transition region (Emslie & Smith 1984), which are proven to be Langmuir waves (Hamilton & Petrosian 1990). The effects of energy losses in Langmuir waves on electron distributions gained in collisional and Ohmic losses for beams with various parameters are presented in Figure 4.

The effect of electric field on electron energy distributions for various depths calculated for energy losses in collisions and Langmuir wave generation is demonstrated in the left column. The distributions simulated for collisions plus waves but without electric field (solid lines) are substantially different from those simulated with electric field (dashed lines). The difference becomes much stronger for more intense beams (compare the plots in the upper and bottom rows). Thus, unlike hydrostatic atmospheres (McClements 1989), the electric field in hydrodynamic atmospheres sharpens electron energy distributions with maxima caused by collisions and reduces the column depths where positive slopes can be formed.

The inclusion of Langmuir waves has a small effect on electron distributions for electron beams with low initial energy fluxes if both collisions and electric field are considered (see dashed plots in the right column in Figure 4), in contrast to those simulated in the absence of Langmuir waves (solid plots). This explains why the consideration of Langmuir turbulence without an electric field can have a small effect on HXR emission produced by moderate beams as found in the previous estimations (Hamilton & Petrosian 1987) and simulations (McClements 1989).

However, for more intense beams with energy fluxes about 10^{12} erg cm^{-2} s^{-1}, the inclusion of Langmuir waves causes a noticeable reduction of electron numbers at lower energies (compare the right plots in the upper and bottom rows). This difference is less noticeable at upper atmospheric levels but becomes bigger at lower ones, which can result in some reduction of the electron numbers deduced from HXR photon counts if Langmuir waves are considered.

3.2.3. Langmuir Waves

As found in Section 3.2.2, the initial single negative power-law velocity distributions of electron beams injected to the ambient plasma are transformed into distributions with a positive slope at lower energies. Electrons with such distributions excite, due to the normal or anomalous Doppler resonance, low- and high-frequency resonant Langmuir oscillations with a phase velocity v_{ph} (Tsytovich 1970).

If Langmuir waves grow in the region where the slope is positive and there is a greater number of faster particles ($v > v_{\mathrm{ph}}$) than slower ones, then a greater amount of energy is transferred from the fast particles to the wave, giving a rise to exponential wave growth with the growth rate γ_w (Tsytovich 1970):

$$\gamma_w \; = \approx \frac{\pi}{2} \frac{n_b}{n} \left(\frac{v_s}{\Delta v_s} \right)^2 \omega_{\mathrm{pe}}, \tag{5}$$

where n_b is the beam density, n is the ambient plasma density, v_s and Δv_s are the mean vertical velocity and the mean spread of this velocity of beam electrons, and ω_{pe} is the electron plasma frequency.

The Langmuir instability grows if the growth rate of waves is greater than the collisional dumping rate γ_{col} defined as (Ginzburg & Zhelezniakov 1958)

$$\gamma_{\mathrm{col}} \approx \frac{5.5n}{T_e^{3/2}} \ln \left(10^4 \frac{T_e^{2/3}}{n^{1/3}} \right) \approx 80 n T_e^{-3/2}, \tag{6}$$

which is appropriate for the coronal values of plasma density n and electron temperature T_e. Thus, the ratio $\Gamma = \frac{\gamma_w}{\gamma_{\mathrm{col}}}$ defines the growth rate of Langmuir waves above the collisional damping, e.g., when $\Gamma \gg 1$, then the waves are most effectively generated.

There are two kinds of beam pairs which can produce the two beam instability and cause Langmuir waves: (1) a direct electron beam and ambient plasma electrons and (2) a direct beam and the beam of returning electrons mixed with the thermal ones. The interaction of the first set of beams on the generation of Langmuir waves throughout precipitation depths from the corona to the chromosphere is presented in the left column of Figure 5 and the effects of the second set including the beam associated with a self-induced electric field are presented in the right column of Figure 5.

At upper atmospheric levels (or at lower column densities, in the corona) the effect of Langmuir waves generated without taking into account electric field effects is clearly noticeable at all the coronal depths for energies below 10 keV for beams with the initial energy flux of $F_0 = 10^{10}$ erg cm^{-2} s^{-1} while shifting to a few tens of keV for the more intense beam ($F_0 = 10^{12}$ erg cm^{-2} s^{-1}). The restriction in energy is likely to occur because only the electrons with energies below or about

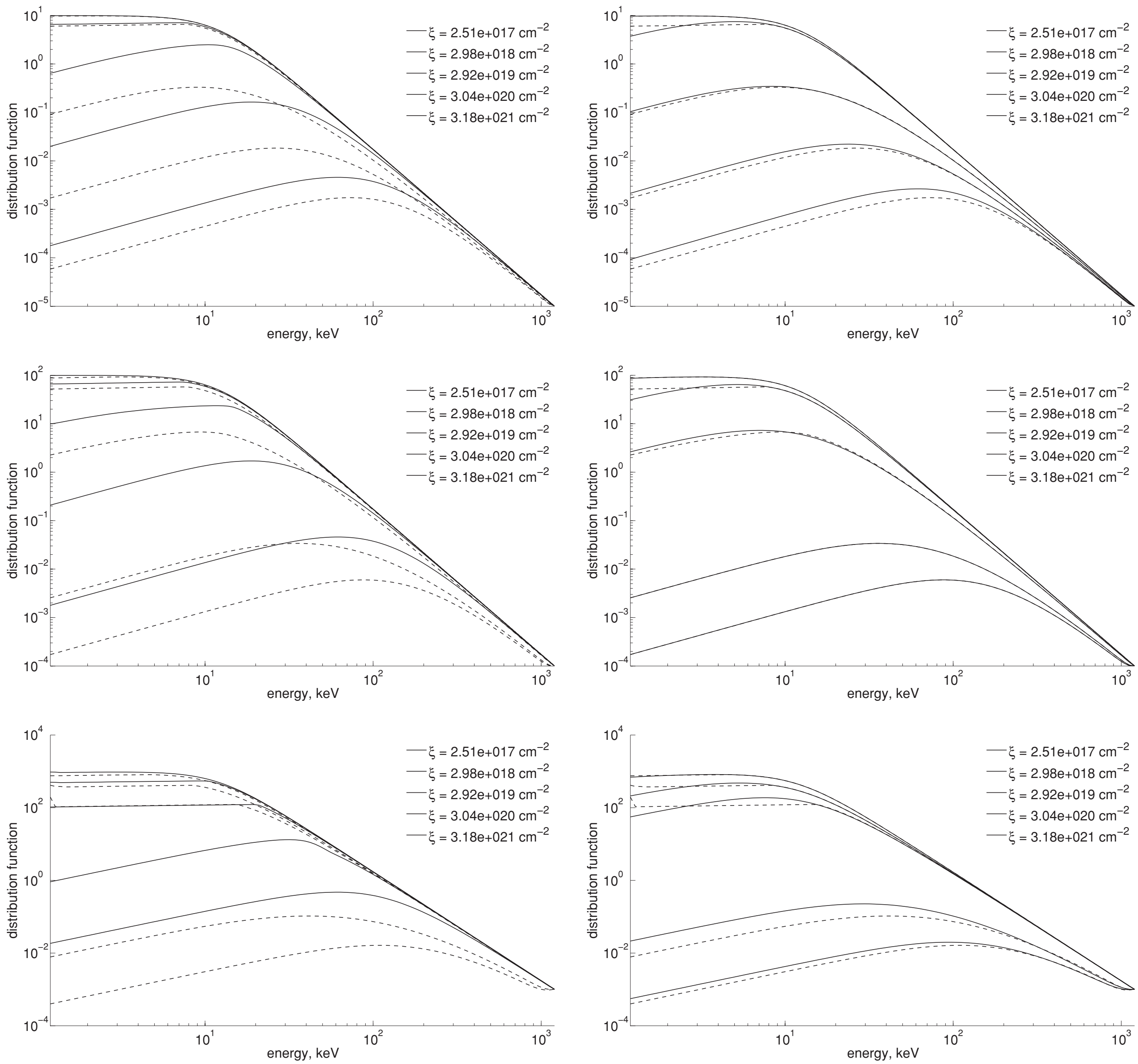

Figure 4. Left column: beam electron distributions (in s cm^{-4}) for collisions and waves but without (solid lines) and with (dashed lines) electric field; right column: beam electron distributions for collisions and electric field without (solid) and with (dashed) Langmuir waves for $F_0 = 10^{10}$ erg cm^{-2} s^{-1} (first row), $F_0 = 10^{11}$ erg cm^{-2} s^{-1} (second row), and $F_0 = 10^{12}$ erg cm^{-2} s^{-1} (third row). The curves are shown from top to bottom for column depths ξ shown in the legend starting from $\xi = 2 \times 10^{17}$ cm^{-2} for the uppermost ones (both solid and dashed).

10 keV are effectively scattered in the corona since the coronal plasma is a thin target (Brown 1971).

There is a sharp peak of wave energy density observed for any beams just below the transition region at about 1×10^{19} cm^{-2} for beams with the initial energy flux of 10^{10} erg cm^{-2} s^{-1} or deeper at 3×10^{19} cm^{-2} and 1×10^{20} cm^{-2} for beams with the initial energy flux of 10^{11} and 10^{12} erg cm^{-2} s^{-1}, respectively. The occurrence of this peak coincides with the peaks in the density and temperature profiles of the ambient plasma heated by beams (Zharkova & Zharkov 2007; see the example in Figure 1). A sharp enhancement in the plasma density and temperature just below the transition region causes an increase of the wave growth rate represented by the second (collisional) term on the right-hand side of Equation (2), which is seen as a peak on Figure 5.

The spread of Langmuir waves at the coronal depths is more extended for beams with energy distributions having higher spectral indices (see the upper left plot in Figure 5) or higher initial energy fluxes (see the bottom left plot in Figure 5). For the beams with the higher initial energy flux of 10^{12} erg cm^{-2} s^{-1} or higher spectral index of 7, the Langmuir wave energy density above the transition region is higher than for a less intense or harder beam.

This occurs because softer beams effectively lose much of their energy in the corona, so that their average velocities v_s, which affect the growth rate of Langmuir waves (see formula (5)), are higher in the corona compared to the chromosphere. Furthermore, the beam density of a softer beam is higher in the corona while the ambient plasma density imposed by a hydrodynamic response (Zharkova & Zharkov 2007) on the

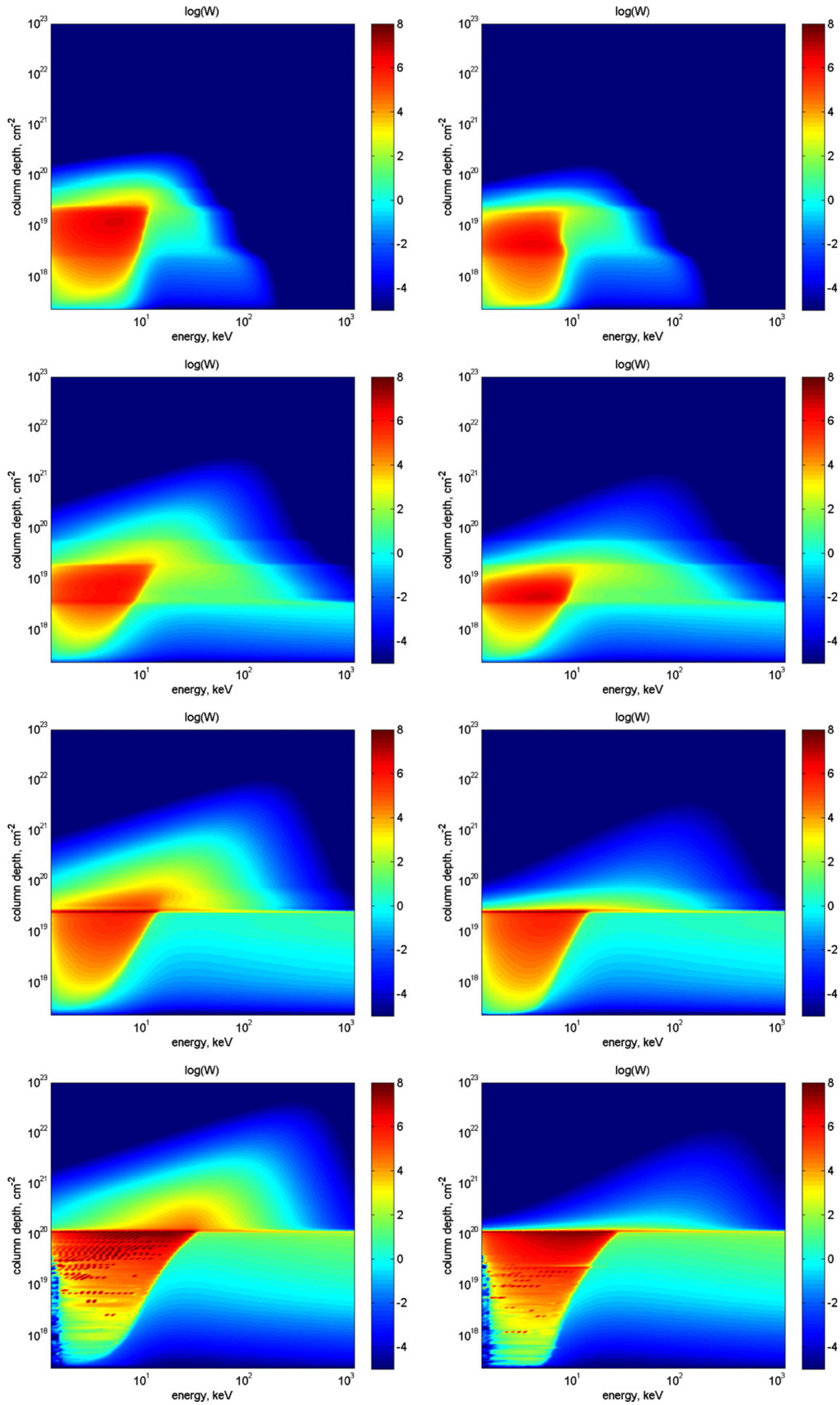

Figure 5. Three-dimensional density of Langmuir wave energy (erg cm^{-4} s) vs. column depth simulated without (left column) and with (right column) a self-induced electric field for the beams with: $\delta = 7$ and $F_0 = 10^{10}$ erg cm^{-2} s^{-1} (first row); $\delta = 3$ and $F_0 = 10^{10}$ erg cm^{-2} s^{-1} (second row); $\delta = 3$ and $F_0 = 10^{11}$ erg cm^{-2} s^{-1} (third row); $\delta = 3$ and $F_0 = 10^{12}$ erg cm^{-2} s^{-1} (fourth row).

(A color version of this figure is available in the online journal.)

beam injection is lower than that for harder beams. This, in turn, increases the Langmuir wave growth rate in the corona. For more intense beams, their total density becomes also higher (from the normalization condition; Siversky & Zharkova 2009b) while the ambient plasma density in the corona becomes much lower than for less intense beams leading again to an increased growth rate of the Langmuir waves (according to formula (5)).

At deeper layers, in the lower corona and in the upper chromosphere, generation of Langmuir waves extends to the electrons with higher energies (two bottom plots in Figure 5). More intense and harder beams produce a more extended region (extended toward the lower chromosphere) where Langmuir waves are generated. Also the wave energy density (color marked in erg cm^{-4} s on the right-hand side of each plot) is higher for such beams compared to weaker or softer beams.

This happens because at the chromospheric depths harder and more intense beams have higher densities and narrower spreads (Δv_s; see formula (5)) compared to softer and weaker beams that again lead to a higher growth rate and denser Langmuir turbulence. However, at these depths collisional damping of the Langmuir waves becomes rather strong resulting in the waves being effectively scattered to larger spatial regions.

However, if the electric field of the beam is considered, the regions with Langmuir waves become smaller. The wave energy peaks move downward to the lower corona in the upper atmosphere (above the depth of the density maximum) and upward to the upper chromosphere (below the depth of the density maximum). The higher the beam's initial energy flux and the lower its spectral index, the narrower the region where Langmuir waves are generated, although the density of these waves becomes higher, i.e., the waves become more intense while localized in a smaller region.

We understand that if the electric field is included, the energy density of Langmuir waves becomes lower at deeper atmospheric levels because of the direct beam density also becoming lower compared to the case with collisions only (see Figure 4). This is caused by a larger number of electrons losing their energy in the upper atmosphere and returning to the injection site on the top with much wider distribution in pitch angles (Zharkova et al. 1995; Siversky & Zharkova 2009b). This significantly reduces the beam density in the chromosphere and thus the Langmuir wave density and spread at these levels.

The effects of an electric field can significantly reduce the intensity of type III MW emission generated by Langmuir turbulence, compared to a collisional case, for which the simulated MW emission intensity in the collisional plus waves model was found to exceed the observed ones by the order of magnitude (Emslie & Smith 1984).

There is another interesting effect derived from the current simulation for very strong beams with the initial flux of 10^{12} erg cm^{-2} s^{-1} appearing for any models (with and without electric field). This is the formation of high-hybrid Langmuir waves in the form of well-defined periodic structures (zebra-type patterns) clearly seen in the bottom plots of Figure 5. The patterns are much more numerous and extend to the whole coronal depths for the model without electric field (the left bottom plot), while they shift to upper coronal levels and have fewer number of patterns for the model with electric field (the right bottom plot).

For the model electron beams with high energy flux and very narrow spread over the pitch angle θ ($\mu = \cos\theta$ is about unity), these periodic oscillations in Langmuir wave generation are believed to be defined by the cyclotron resonance of beam electrons with the derived distributions. Electrons with such velocity distributions can also excite, due to the anomalous Doppler resonance, resonant Langmuir oscillations with frequencies $\omega_2 = \min(\omega_{pe}, \omega_{He})$, where ω_{pe} and ω_{He} are the electron plasma and gyrofrequencies (see discussion in Kovalev 2009).

Low- and high-frequency modes of Langmuir oscillations form high-amplitude periodic nonlinear waves seen as well-defined patterns in the bottom plots of Figure 5. The inclusion of an electric field significantly increases the spread of the electron beam (Zharkova et al. 1995; Siversky & Zharkova 2009b) that substantially reduced the growth rate for Langmuir waves, in general, and for high-hybrid Langmuir waves, in particular, as shown in the bottom left plot of Figure 5.

The corresponding spectrum of electromagnetic waves excited resonantly by the current of potential waves can also form an equidistant spectrum of electromagnetic radio radiation in the plasma or zebra structure. This structure can account for the generation of the "zebra-"type IV MW bursts (Chernov 2006) often observed in flares.

4. CONCLUSIONS

In the current study, we have compared the effects of collisional and Ohmic energy losses of beam electrons with those caused by the electron energy exchange with Langmuir waves generated by the beams during their precipitation into hydrodynamic atmospheres.

The beams with a positive slope in the initial energy distribution reveal a fast flattening of their energy spectra on a very short spatial and temporal scale, which is caused by the formation of Langmuir waves and their suppression by a strong self-induced electric field.

The precipitation of beam electrons into a flaring atmosphere with density and temperature gradients results in transformation of electron energy/velocity distributions at some depths into the distributions with maximums, which have positive slopes for energies below these maximums and still have negative power laws for energies above it (Syrovatskii & Shmeleva 1972; Emslie & Smith 1984).

High energy electrons with velocity distributions having positive slopes, gained during their precipitation, can also excite low- and high-frequency resonant Langmuir waves. At upper atmospheric levels, in the corona, the generation of Langmuir waves affects the electrons with energies below 10 keV for weak beams and below a few tens of keV for the most intense ones. The energy density of Langmuir waves at these levels is higher for softer or more intense beams.

Also there is a sharp peak in Langmuir wave density observed for any beams at about 10^{19} cm^{-2} for beams with the initial energy flux of $F_0 = 10^{10}$ erg cm^{-2} s^{-1} which moves into a deeper level of 10^{20} cm^{-2} for beams with the initial energy flux of $F_0 = 10^{12}$ erg cm^{-2} s^{-1}. The occurrence of this peak coincides with peaks in the density and temperature profiles of the ambient plasma, which shift much deeper into the chromosphere for more intense beams.

At deeper layers, in the lower corona and in the upper chromosphere, the generation of Langmuir waves extends to the electrons with higher energies up to 100 keV. More intense and harder beams produce more extended region toward the lower chromosphere where Langmuir waves are generated. Also, the wave energy density is higher for more intense and harder beams.

The inclusion of a self-induced electric field, in addition to collisions, into the energy losses by beam electrons is shown to decrease the depths where the distributions with maxima are formed and increase the energy of these maxima. This in turn increases the number of beam electrons at upper atmospheric levels, in the corona, and decreases it in the chromosphere, in comparison to those deduced for purely collisional precipitation.

As a result, our simulations show that, contrary to the previous findings (McClements 1989), if the energy losses in a self-induced electric field are included, in addition to collisions, the Langmuir waves are found to appear in a much narrower space than in the collisional plus wave models and have a narrower energy range. In the presence of electric field, the region with Langmuir waves in the corona is also shifted downward to the lower corona, while in the chromosphere it is shifted upward to the upper chromosphere.

The higher the beam initial energy flux and the lower the spectral index, the narrower the regions where Langmuir waves are generated. The density of these waves becomes higher, i.e., the waves become more intense. Therefore, the electric field of an electron beam plays a very important role in suppressing the generation of Langmuir turbulence at all atmospheric levels by reducing the spread and increasing the density of these waves in all the atmospheric depths above and below the transition region.

The effects of electric field can significantly reduce the intensity of type III MW emission generated by Langmuir turbulence, compared to the collisional plus waves case, for which the simulated MW emission intensity in the collisional plus waves model was found to exceed the observed ones by the order of magnitude (Emslie & Smith 1984).

Additionally, very distinct patterns of high-hybrid Langmuir waves are found to be generated by electrons from very strong beams in the form of well-defined periodic (zebra-type) structures. They occur in the coronal part of the atmosphere and have a limited number of patterns for both parameters: atmospheric depth and electron energy.

The inclusion of a self-induced electric field reduces the number of these patterns in energy and in depth leading to their occurrences shifting to higher atmospheric levels in the corona and higher energies. These structures can be accountable for the zebra patterns observed in the type IV MW bursts.

The authors thank the anonymous referee for very constructive and useful comments from which the paper strongly benefited. This research was partially funded by the Science Technology and Facility Council (STFC) project PP/E001246/1 and the Royal Society Joint International Grant with the Institute of the Solar-Terrestrial Physics, Irkutsk, Russian Federation.

REFERENCES

Brown, J. C. 1971, Sol. Phys., 18, 489
Chernov, G. P. 2006, Space Sci. Rev., 127, 195
Diakonov, S. V., & Somov, B. V. 1988, Sol. Phys., 116, 119
Emslie, A. G. 1980, ApJ, 235, 1055
Emslie, A. G., & Smith, D. F. 1984, ApJ, 279, 882
Ginzburg, V. L., & Zhelezniakov, V. V. 1958, SvA, 2, 653
Hamilton, R. J., & Petrosian, V. 1987, ApJ, 321, 721
Hamilton, R. J., & Petrosian, V. 1990, ApJ, 365, 778
Hannah, I. G., Kontar, E. P., & Sirenko, O. K. 2009, ApJ, 707, L45
Karlický, M., Nickeler, D. H., & Bárta, M. 2008, A&A, 486, 325
Knight, J. W., & Sturrock, P. A. 1977, ApJ, 218, 306
Kovalev, V. A. 2009, Plasma Phys. Rep., 35, 394
Leach, J., & Petrosian, V. 1981, ApJ, 251, 781
McClements, K. G. 1987, A&A, 175, 255
McClements, K. G. 1989, A&A, 208, 279
McClements, K. G. 1992, A&A, 258, 542
Siversky, T. V., & Zharkova, V. V. 2009a, J. Plasma Phys., 75, 619
Siversky, T. V., & Zharkova, V. V. 2009b, A&A, 504, 1057
Somov, B. V., Spektor, A. R., & Syrovatskii, S. I. 1981, Sol. Phys., 73, 145
Syrovatskii, S. I., & Shmeleva, O. P. 1972, SvA, 16, 273
Tsytovich, V. N. (ed.) 1970, Nonlinear Effects in Plasma (New York: Plenum)
Zharkova, V. V., Brown, J. C., & Syniavskii, D. V. 1995, A&A, 304, 284
Zharkova, V. V., & Gordovskyy, M. 2005, MNRAS, 356, 1107
Zharkova, V. V., & Gordovskyy, M. 2006, ApJ, 651, 553
Zharkova, V. V., Kuznetsov, A. A., & Siversky, T. V. 2010, A&A, 512, A8
Zharkova, V. V., & Zharkov, S. I. 2007, ApJ, 664, 573
Zheleznyakov, V. V., & Zaitsev, V. V. 1970, SvA, 14, 47